The International Journal of Advanced Manufacturing Technology (2023) 125:3037–3051
https://doi.org/10.1007/s00170-023-10867-7

ORIGINAL ARTICLE

Criterion and processing-dependence of forming states in the die-less spinning of conical part

Xinggang Yan[1] · Mei Zhan[1] · Yao Wang[1] · Pengfei Gao[1] · Yongdi Wang[1]

Received: 4 August 2022 / Accepted: 11 January 2023 / Published online: 28 January 2023

Abstract

In the die-less spinning of the conical part, the forming state changes during the spinning process and depends on the forming parameters, which has a critical effect on the forming quality of the spun part. In this paper, a criterion of the forming states is established, and its dependence on the forming parameters is investigated. It is found that the formed wall thickness changes during die-less spinning. According to the formed wall thickness variation degree, three forming states are defined: shear spinning state ($t_f = t_0 sin\alpha$, where t_0 and t_f are the initial and formed wall thicknesses, respectively, and α is half-cone angel), the conventional spinning state ($t_f > 0.9t_0$), and transition state between the shear and conventional spinning states ($t_0 sin\alpha < t_f \leq 0.9t_0$). The distribution of stress and strain in three forming states is obviously different. The die-less spinning always proceeds in the sequence of shear spinning state, transition state, and conventional spinning state. The initial forming state may be any one of them, which is mainly determined by the diameters of the blank and general mandrel. Thus, the quantitative dependence of initial forming state on the diameters of blank and general mandrel is further analyzed, and a criterion for the initial forming state is correspondingly established. In addition, the influence of forming parameters, including the blank parameters, mold parameters, and process parameters, on the criterion for the initial forming state in die-less spinning is revealed. This paper could improve the understanding of the deformation mechanism in die-less spinning.

Keywords Die-less spinning · Forming state · Criterion · Forming parameters dependence

1 Introduction

The complex thin-walled axisymmetric part, such as the conical part, is a critical component in aerospace and automotive industries. To satisfy the forming requirements of high performance and high precision, it is necessary to develop a precise and effective forming method for this kind of part. Spinning has become the main forming process of these parts due to its advantages of low forming load, simple tools, high forming precision, and good surface finish [1–3]. As a typical local loading plastic forming process, the spinning process forms parts by rollers' pression on the rotating workpiece, where the workpiece is driven to rotate by the mandrel. The spinning could be divided into mandrel spinning (Fig. 1a) and die-less spinning (Fig. 1b) according to the type of mandrel. Mandrel spinning has a customized mandrel whose shape and dimension are same as those of the target component. In contrast, a general mandrel is used to fix the workpiece in die-less spinning, and this simple equipment makes the die-less spinning used widely [4].

In the mandrel spinning, the blank is deformed under the constraint of mandrel, and the wall thickness reduces according to the gap between the mandrel and roller, which usually obeys the sine-law reduction [5–7]. Compared with the mandrel spinning process, the die-less spinning presents more complex wall thickness variation and stress–strain state due to the lack of customized mandrel constraints [8]. Many researchers [9–11] have investigated the variation of wall thickness during the spinning process and found that the wall thickness variation gradually increases from a sine-law reduction to no-reduction, and even thickens at the end in die-less spinning. This leads to the non-uniform

✉ Mei Zhan
zhanmei@nwpu.edu.cn

✉ Pengfei Gao
gaopengfei@nwpu.edu.cn

[1] State Key Laboratory of Solidification Processing, Shaanxi Key Laboratory of High-Performance Precision Forming Technology and Equipment, School of Materials Science and Engineering, Northwestern Polytechnical University, Xi'an 710072, People's Republic of China

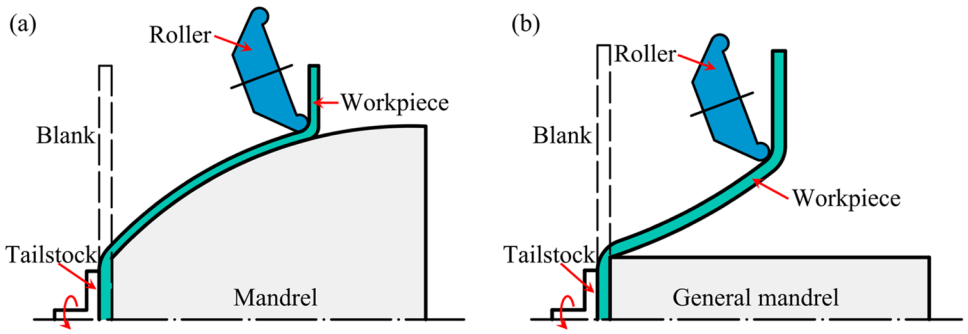

Fig. 1 Schematics of mandrel spinning (**a**) and die-less spinning (**b**)

distribution of wall thickness in the radial direction of the formed workpiece.

The complex variation of formed wall thickness indicates that there are different forming states presenting various stress–strain distributions during die-less spinning. Wang et al. [9] found that there was a complex distribution of stress–strain in die-less spinning. Furthermore, Gondo [12] studied the distribution of stress and strain during die-less spinning of cylindrical cups and defined four strain states and their corresponding stress characteristics. Generally, the forming quality is greatly dependent on the forming state in the die-less spinning [13]. For example, the wrinkles in die-less spinning are caused mainly by circumferential compressive stress in the flange area [14]; the wall thickness variation is determined by the strain state in the forming area [8]. Therefore, to improve the forming quality of the spun part, it is important to determine the variation law of forming states and their processing dependence. Kang et al. [15] have found that the forming states were related to the width of flange area in the die-less spinning. However, there is still a lack of quantitative criterion for the forming state and its dependence on the forming parameters.

In this paper, three forming states in die-less spinning are defined in detail, and the corresponding distribution of stress and strain is studied. Furthermore, the evolution of forming states during the spinning process is revealed. On this basis, the criterion of forming states for die-less spinning is established, and the influence of forming parameters on the forming states criterion is analyzed.

2 Experimental investigation and finite element simulation for the die-less spinning

2.1 Die-less spinning experiment

All physical die-less spinning experiments are performed on a CZ900/2CNC spinning machine (Fig. 2) in this study. The material used in the die-less spinning experiment is the

Fig. 2 CZ900/2CNC multi-function spinning machine with double rollers

Table 1 Mechanical properties of 1060-O aluminum

Young's modulus/GPa	Poisson's ratio	Yield strength/MPa	Tensile strength/MPa	Hardening index (n)	Strengthening coefficient (K)/MPa
71.70	0.33	30.85	75.00	0.17748	93.94

1060-O aluminum alloy plate with a thickness of 1 mm. The deformation stress–strain curve of the material is measured by the uniaxial tensile tests at room temperature using the CMT5205 universal testing machine. The stress–strain relationship is described by the Hollomon equation $\sigma = K\varepsilon^n$. The detailed mechanical properties and constitutive equation parameters are shown in Table 1.

Three typical blanks with diameters of 114, 136 and 220 mm are selected to perform the die-less spinning experiments. The initial blank is tied to the general mandrel by a bolt during the die-less spinning process, so that it can rotate by the driving of the general mandrel. In order to form the conical part, two rollers distribute symmetrically and feed along a straight line with the half cone angle of 50°. The diameters of the rollers and mandrel are 250 mm and 90 mm, respectively. The corner

radius of rollers and mandrel are 4 mm and 10 mm, respectively. In addition, the mounting angle of rollers is 30°, and the rotating speed of the general mandrel is set as 60 r/min. Under this condition, the formed shape and wall thickness distribution of three typical blanks are shown in Fig. 3.

2.2 Finite element simulation

In this paper, FE simulations for die-less spinning are carried out on the ABAQUS platform. Considering that the spinning is a nonlinear and dynamic process with complex contact conditions, the Explicit Solver based on the

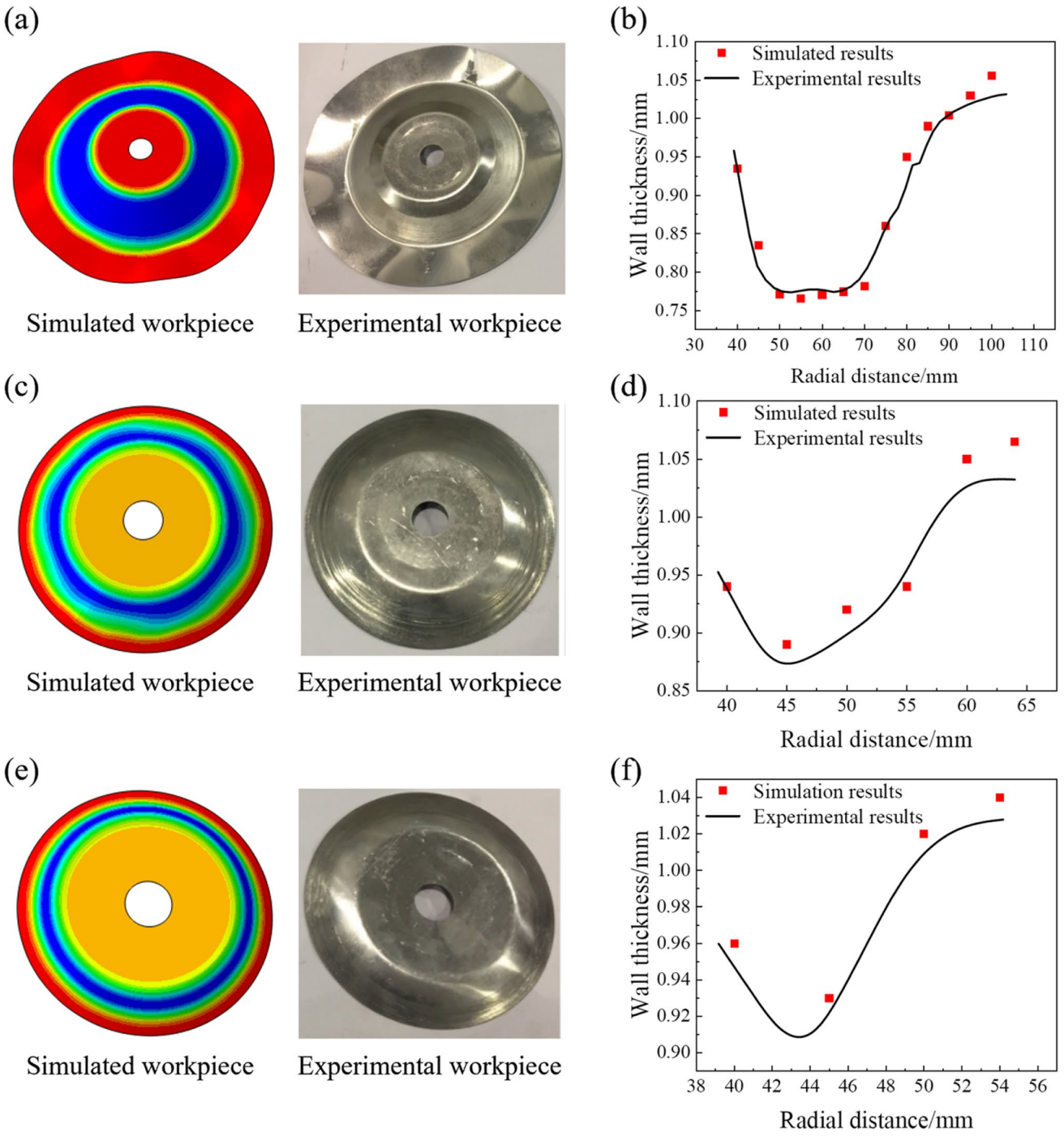

Fig. 3 Comparison of formed shape (**a**, **c**, **e**) and wall thickness (**b**, **d**, **f**) between the simulated and experimental workpieces with the initial diameters of: **a**, **b** 220 mm; **c**, **d** 136 mm; **e**, **f** 114 mm (Radial distance in **b**, **d**, **f** means that the distance between the measuring points and symmetrical axis of the blank)

dynamic explicit algorithm is employed to simulate the spinning process. In the simulation model, the blank is set as the deformable part, while the rollers and general mandrel are set as the discrete rigid part. The dimension and assembly of the blank and tools remain the same as those of the physical experiment, and the assembly relationship is shown in Fig. 4a. To simplify the FE model, a coupling constrict is used to tie the blank to the general mandrel instead of a bolt. The material is considered to be homogeneous and elastoplastic, and the elastic stage is described by Hooke's law; the plastic stage is described by the Hollomon equation according to Table 1. To describe the dynamic contact, two roller-blank contact pairs are defined using the surface-to-surface contact type and penalty function algorithm, and the friction coefficient is set as 0.05 [8]. Using the sweep technique, the blank is discretized by four-node doubly curved thin quadrilateral shell reduced integral elements (S4R) with hourglass enhanced control in the FE model. Moreover, the mass scaling factor is set as 2000 to accelerate model computing.

To determine the appropriate mesh size, the FE models with different mesh sizes are established and simulated. The blank diameter is selected as 220 mm, and the circumferential-radial size ratio ranges from 0.3 to 3. The detailed radial mesh sizes are listed in Table 2. After simulations, the simulated wall thickness distributions and the maximum relative errors are gathered and presented as Fig. 5. The differences of wall thickness between the FE models and experiment decrease with the decrease of mesh size. When the radial mesh size is smaller than 2.5 mm, the wall thickness distributions of the FE models are very close and agree well with the experimental results. So the mesh size in this study is selected as 2 mm in radial direction and 0.6–6 mm in circumferential direction (Fig. 4b).

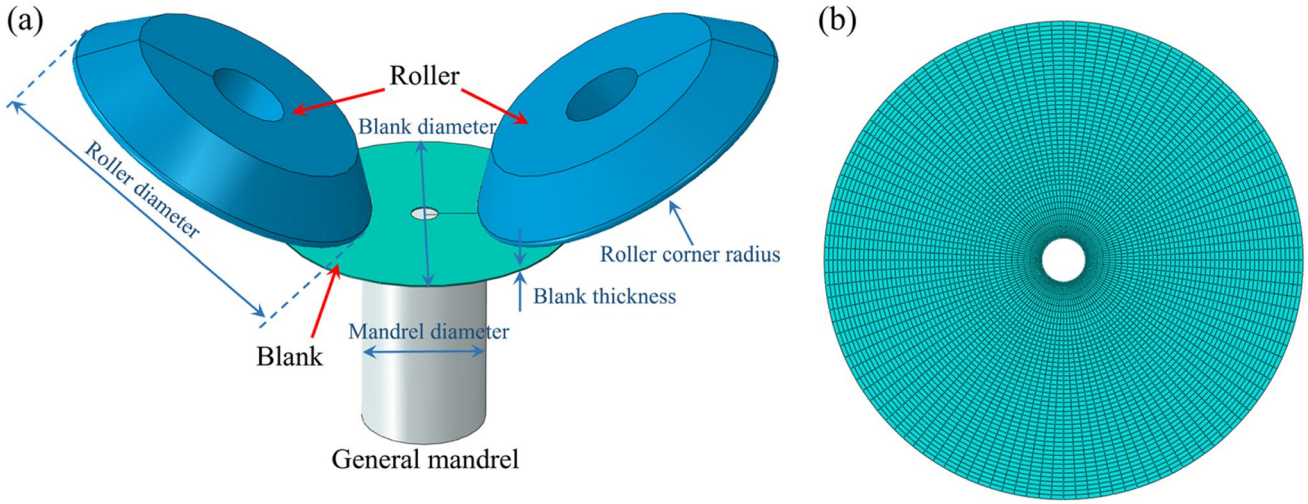

Fig. 4 Schematics of three-dimensional finite element model for the die-less spinning process: (**a**) assembly relationship; (**b**) blank mesh

Table 2 Mesh sizes of different FE models

	Model 1	Model 2	Model 3	Model 4	Model 5	Model 6
Radial size	1.5	2	2.5	3	3.5	5

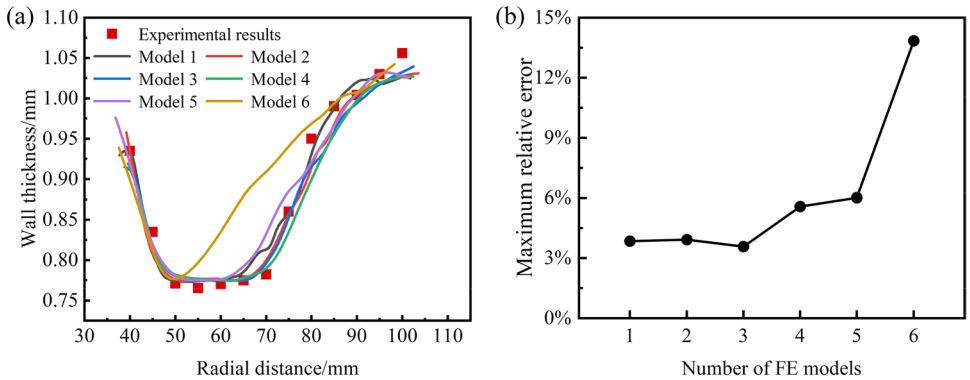

Fig. 5 The wall thickness distributions (**a**) and the maximum relative errors (**b**) of FE models with different mesh sizes

To verify the rationality and accuracy of the FE model, FE model simulations of three typical blanks are carried out, and the dimensions of typical blanks are the same as that of physical experiment in Sect. 2.1. The verification of the FE model is conducted in terms of energy balance and geometric similarity. Generally, the simulation is regarded as a steady process when the kinetic energy of the workpiece is less than 10% of the internal energy, and there will be no unreasonable deformation caused by the hourglass problem when the artificial strain energy of the workpiece is less than 5% of the internal energy. As a representative sample, the energy variation in the die-less spinning process of the blank with a diameter of 220 mm is shown in Fig. 6. It can be found that both the ratio of kinetic energy to internal energy and the ratio of artificial strain energy to internal energy are less than the critical value during most of the die-less spinning, which illustrates that the FE model is acceptable in terms of energy balance.

Moreover, the comparisons of formed shape and wall thickness between the simulation and experiment of three typical blanks are shown in Fig. 3. There is great shape similarity between the simulation and experimental workpieces. The maximum relative errors of formed wall thickness between the FE model and physical experiment are 3.9% for the blank with a diameter of 220 mm, 3.2% for the blank with a diameter of 136 mm, and 1.4% for the blank with a diameter of 114 mm, respectively. These results indicate that the FE model could well predict the experimental result during the die-less spinning process. Therefore, the FE model could be used to analyze the deformation characteristics in the die-less spinning.

3 Results and discussion

3.1 Forming states in the die-less spinning

Figure 7 shows the variation of formed wall thickness with forming time in the spinning of the three typical blanks mentioned in Sect. 2.1. It is obvious that there are similar trends in the thickness variation of the three typical blanks. Their formed wall thicknesses all decrease first and subsequently increase to a value larger than the initial value, but the minimum formed wall thickness and the corresponding time are different among the three typical blanks. For the blank with 114 mm diameter, the formed wall thickness decreases to the minimum value of 0.91 mm at 19 s; the formed wall thickness of the blank with 136 mm diameter decreases to the minimum value of 0.87 mm at 20 s; the formed wall thickness of the blank with 220 mm diameter decreases to the minimum value of 0.77 mm at 26 s. The reason why the wall thickness decreased at the beginning of the spinning process is that the rollers gradually come into contact with the workpiece and reach the predefined path. This stage is defined as unstable stage and will not be considered in the following analyses.

The formed wall thickness variation is determined by the strain states in die-less spinning and driven by the stress states. Thus, to analyze the variation of formed wall

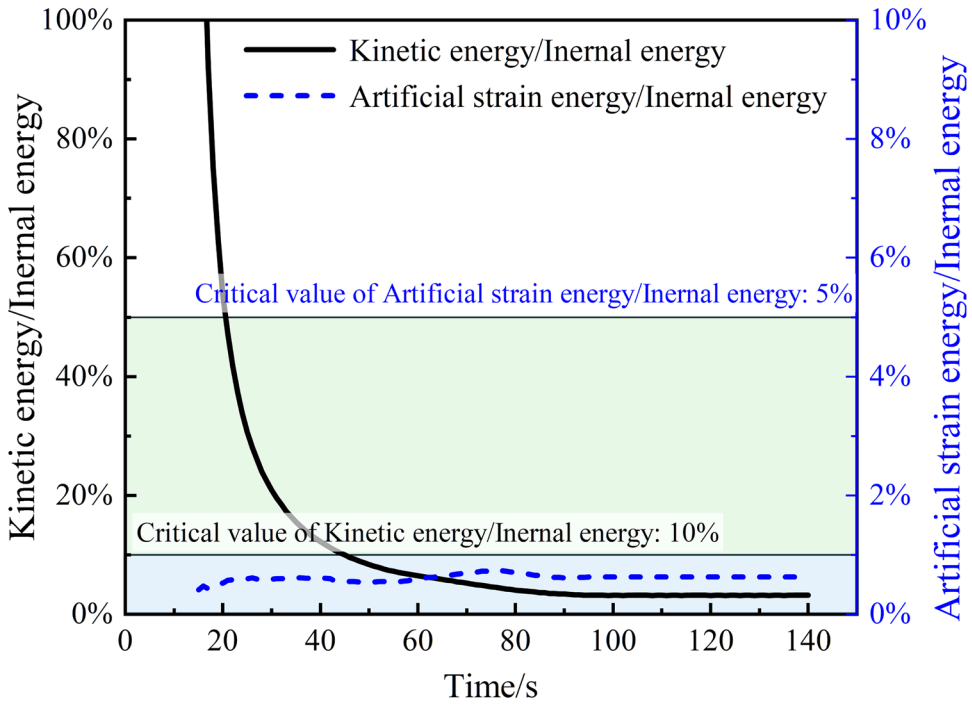

Fig. 6 Energy variation during the die-less spinning process of the blank with diameter of 220 mm

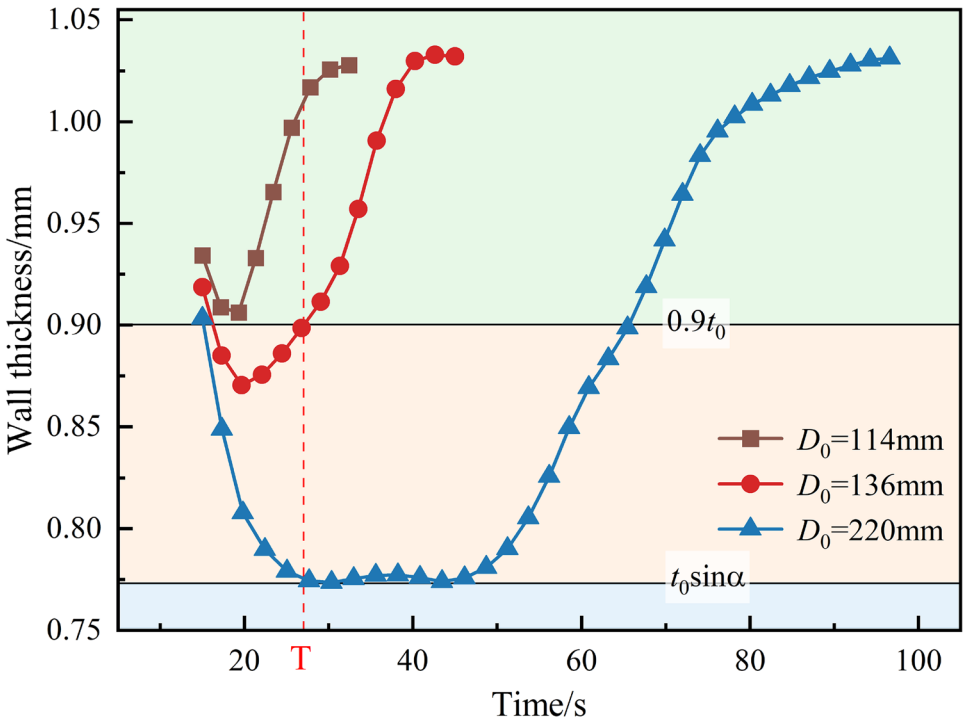

Fig. 7 Variation of the formed wall thickness with forming time of three typical blanks (t_0 is the wall thickness of initial blank; α is half-cone angel; D_0 is the diameter of initial blank)

thickness, it is necessary to determine the distribution of stress and strain. According to the position of rollers, the spinning workpiece can be divided into three characteristic areas: the formed area, roller action area, and flange area (Fig. 8a). Considering that the main deformation occurs in the roller action area, the radial path containing the roller action area (Fig. 8b) is chosen to analyze the distribution of stress and strain. The results of stress and strain will be gathered at the nodes selected along this path at interval of 2 mm.

The distribution of stress and strain in the radial path at time $T = 23.5$ s (noted in Fig. 7) of three typical blanks is shown in Figs. 9 and 10. It can be seen from Fig. 9a that the equivalent stress distribution has a similar trend along the radius path for three typical blanks: the equivalent stress increases in the formed area and then decreases in the roller action area and flange area. However, the stress components greatly vary in the three spinning processes. For the spinning process of the blank with a diameter of 114 mm, the constraint of the flange area to the roller action area is small due to the small rigidity of the flange, so the workpiece undergoes a high-level compressive stress in the roller action area and flange area under the pression of rollers. In contrast, both the radial stress and circumferential stress of the blank with a diameter of 220 mm present positive in the roller action area and remain a low level in the flange area. This is because the rigidity of the flange is big enough to constrain the roller action area, and thus, the flange provides a radial

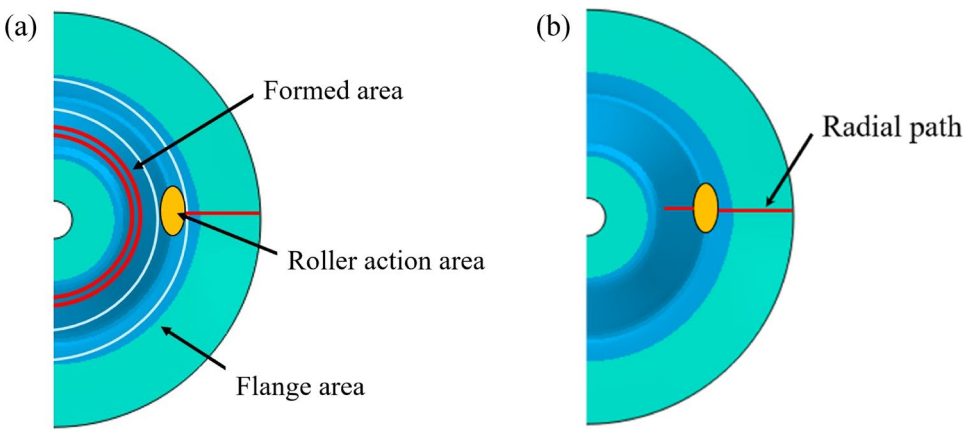

Fig. 8 Schematic diagram of area partitions (**a**) and radial path (**b**)

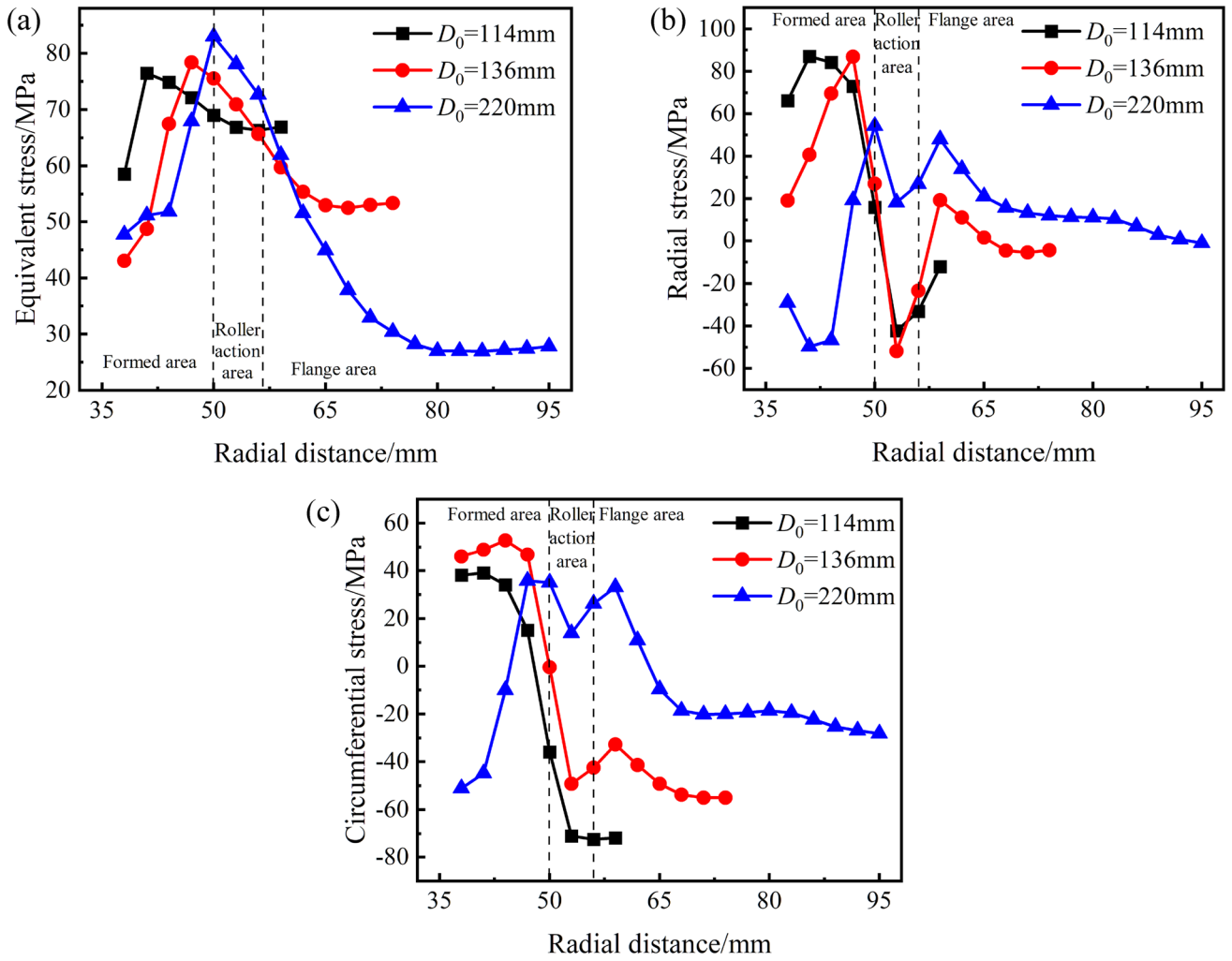

Fig. 9 Stress distribution during the spinning processes of three typical blanks: **a** equivalent stress; **b** radial stress; **c** circumferential stress

tensile stress in the boundary between the roller action area and flange area [8, 15]. The radial compression amount of the blank with a diameter of 136 mm is between that of the blanks with diameters of 114 mm and 220 mm, leading that the absolute value of radial stress and circumferential stress is between that of the blank with diameters of 114 and 220 mm.

Figure 10 shows the distribution of equivalent, radial, circumferential, thickness and second principle strains during the spinning processes of three typical blanks. The roller action area and formed area of the blank with a diameter of 220 mm undergo severe radial tensile deformation and thickness compressive deformation, as well as slight circumferential deformation. As a result, the equivalent strain is much greater than that of the blanks with diameters of 114 mm and 136 mm. The severe equivalent strain of the blank with a diameter of 220 mm stems from the high equivalent stress in the roller action area (Fig. 9). However, the flange area presents almost no deformation. This could be explained by the fact that the deformation mode in the roller action area is simple shear deformation in the plane of thickness and radial directions (which can be verified by that its second principle strain is near to zero in Fig. 10e), and thus, there is almost no radial displacement and deformation occurring in the flange area of the blank with a diameter of 220 mm. As for the blanks with diameters of 114 mm and 136 mm, there is little radial and thickness deformation, as well as obvious circumferential deformation in the roller action area and flange area.

The above analyses indicate that the distribution of stress and strain greatly influence the formed wall thickness variation. It is obvious that there are three typical kinds of distribution characteristic of stress, strain, and thickness:

1. For the spinning process of the blank with a diameter of 114 mm, the workpiece undergoes a high-level compressive stress in the radial and circumferential direction of the roller action area and flange area. There is little radial and thickness deformation, as well as large cir-

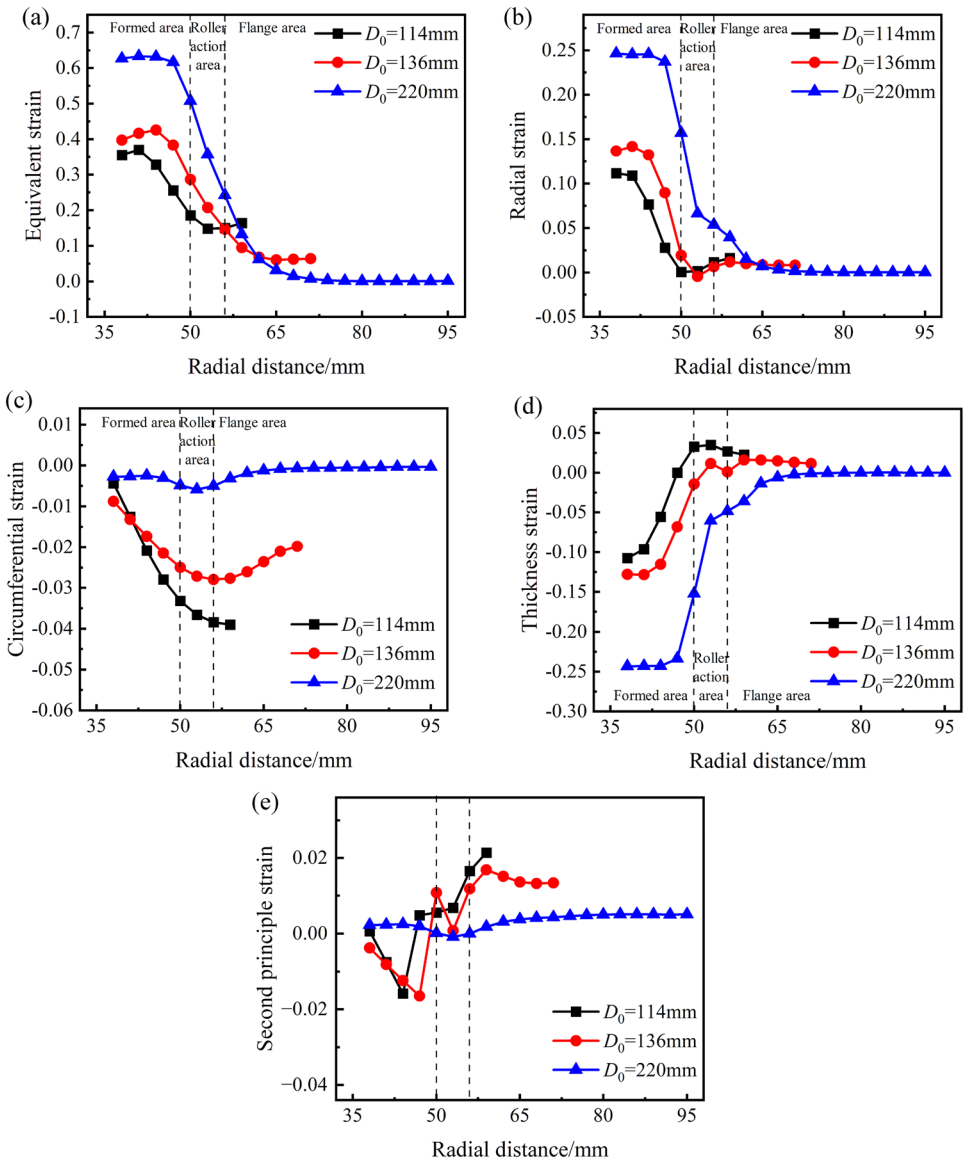

Fig. 10 Strain distribution during spinning processes of three typical blanks: **a** equivalent strain; **b** radial strain; **c** circumferential strain; **d** thickness strain; **e** second principle strain

cumferential deformation, in the roller action area and flange area. The formed wall thickness reduction is less than 10%. The above characteristics are similar as those in the conventional spinning, so this state is defined as conventional spinning state, which can be distinguished by $t_f > 0.9t_0$.

2. For the spinning process of the blank with a diameter of 220 mm, the workpiece undergoes a positive radial and circumferential stress in the roller action area and a low-level radial and circumferential stress in the flange area. The roller action area undergoes severe radial tensile deformation and thickness compressive deformation, as well as slight circumferential deformation, and the deformation of the flange is near to zero. The formed wall thickness reduction is equal to sine-law reduction. The above characteristics is similar as those in the shear spinning, so this state is defined as shear spinning state, which can be distinguished by $t_f = t_0 sin\alpha$.
3. The stress, strain, and thickness characteristic of the blank with a diameter of 136 mm is between the conventional state and shear state, so this state is defined as transition state between shear and conventional spinning state (hereinafter referred to as "transition state"), which can be distinguished by $t_0 sin\alpha < t_f \leq 0.9t_0$.

Apart from the different formed wall thickness variations, the different forming states will also give rise to different tendencies of forming defects. For example, wrinkles in die-less spinning could be caused by large circumferential compressive stress in the flange area [14]. Combining the stress and strain characteristics, the shear spinning state is less likely to wrinkle, and the conventional spinning state

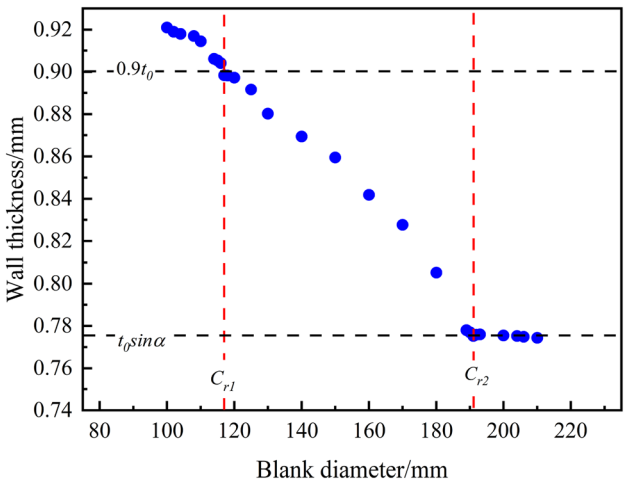

Fig. 11 Variation in formed wall thickness at the initial forming state with different blank diameters

has the greatest possibility to wrinkle. Therefore, determining the evolution law of forming states is critical to improve forming quality.

Based on the definition of forming states, it can be concluded that the spinning process with the blank diameter of 114 mm undergoes the conventional spinning state all the time; the spinning process with the blank diameter of 136 mm contains transition state and conventional spinning state, and spinning process with the blank diameter of 220 mm undergoes all the three states. Furthermore, in order to describe the state evolution clearly and convenient, the forming state after unstable stage (forming state when the wall thickness reaches a minimum value) is defined as the initial forming state. Thus, the initial forming states of three spinning processes are the conventional spinning state, transition state, and shear spinning state, respectively. It can be found that the evolution of forming states during the die-less spinning process can be determined by the initial forming state. When the initial forming state is conventional spinning state, the spinning process will always be under the conventional spinning state; when initial forming state is transition state, the spinning process will contain the transition state and conventional spinning state; and the spinning process will undergo shear spinning state, transition state, and conventional state when the initial forming state is shear spinning state. It is of great significance to determine the initial forming state in a die-less spinning process; thus, the criterion for the initial forming state will be determined in the next section.

3.2 Development of criterion for the initial forming state

The results in Sect. 3.1 suggest that there is a strong link between the blank diameter and initial forming states criterion. Meanwhile, Kang et al. [16] revealed that both the blank diameter and general mandrel diameter contribute to formed wall thickness reduction during the die-less spinning

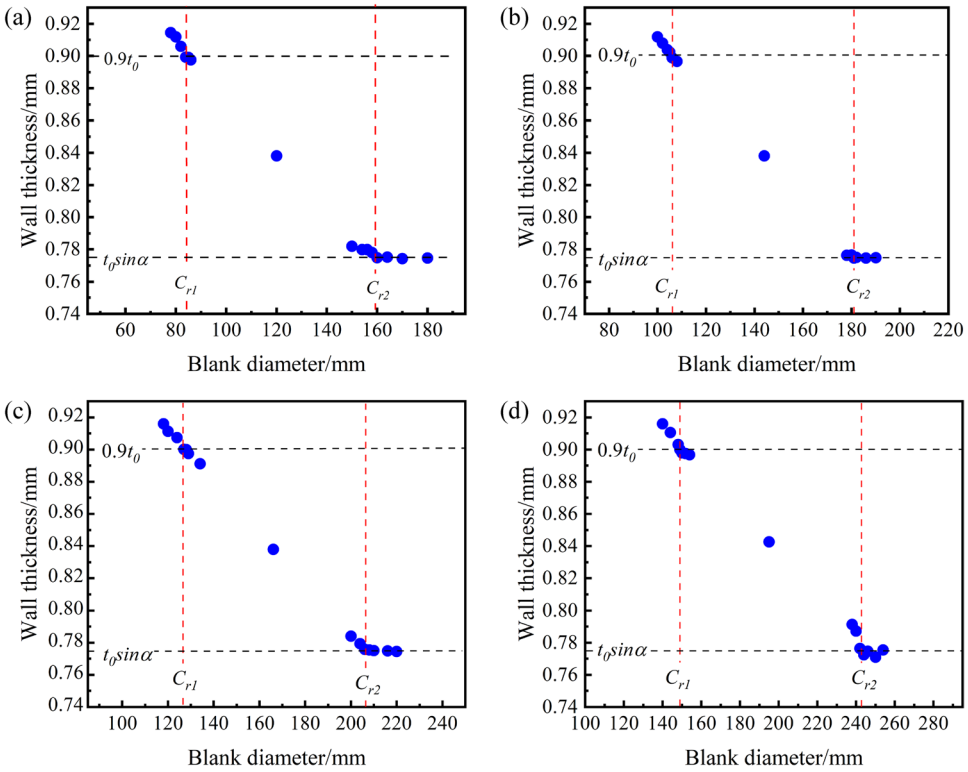

Fig. 12 Variation in formed wall thickness at the initial forming state with blank diameter under different mandrel diameters: **a** 60 mm; **b** 80 mm; **c** 100 mm; **d** 120 mm

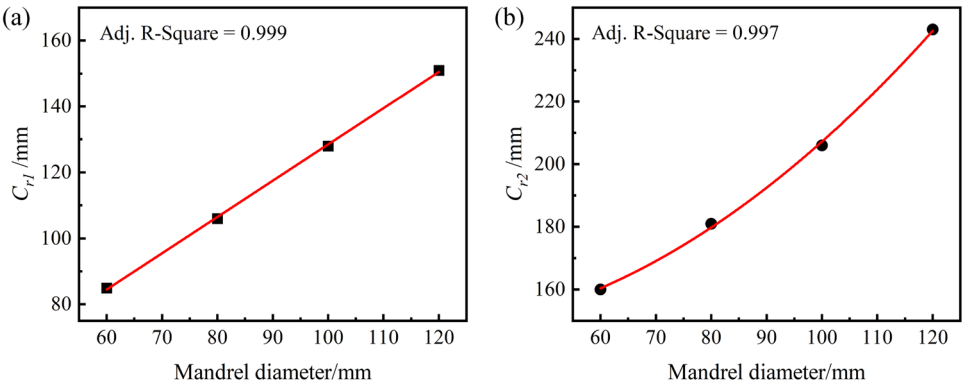

Fig. 13 Variations of C_{r1} (**a**) and C_{r2} (**b**) with the diameter of general mandrel

process. Therefore, the blank diameter and general mandrel diameter are selected as the key parameters to establish the criterion for the initial forming state. And the criterion contains two parts: the critical blank diameter between the conventional spinning state and transition state (noted as C_{r1}) at a certain mandrel diameter and the critical blank diameter between the transition state and shear spinning state (noted as C_{r2}) at a certain mandrel diameter.

In order to determine C_{r1} and C_{r2}, a series of single-factor simulations are conducted based on the FE model developed in Sect. 2.2. The range of blank diameter is set as 100–220 mm, and a smaller interval is used when the blank diameter is near the critical value. Figure 11 shows the relationship between the formed wall thickness at the initial forming state and blank diameter when the general mandrel diameter is 90 mm. It can be seen that the formed wall thickness at the initial forming state decreases monotonically and then keeps at sine-law reduction value with increasing blank diameter. The formed wall thickness is larger than $0.9t_0$ when the blank diameter is less than 117 mm, and the formed wall thickness variation rate is equal to $sin\alpha$ when the blank diameter is greater than 191 mm. Therefore, the criteria C_{r1} and C_{r2} are determined to be 117 mm and 191 mm, respectively.

Similarly, four groups of simulations are conducted to determine the C_{r1} and C_{r2} when the diameter of the general mandrel is 60, 80, 100, and 120 mm, respectively. Figure 12 shows the results of the variation of the formed wall thickness at the initial forming state with the blank diameter under different mandrel diameters. The variation trends of formed wall thickness at the initial forming state in Fig. 12 are the same as those under general mandrel diameter of 90 mm in Fig. 11.

The critical blank diameters C_{r1} and C_{r2} under different general mandrel diameters are shown in Fig. 13. It can be seen that both C_{r1} and C_{r2} increase with increasing general mandrel diameter. However, there is a difference in the increasing rate of C_{r1} and C_{r2}: the critical value C_{r1} increases linearly with increasing general mandrel diameter, while the increase curve of C_{r2} with the general mandrel diameter is

Table 3 Comparison of critical values between measurements and predictions

	C_{r1}/mm	C_{r2}/mm
Measurements	117	191
Prediction	117.5	192.5
Error (%)	0.43	0.78

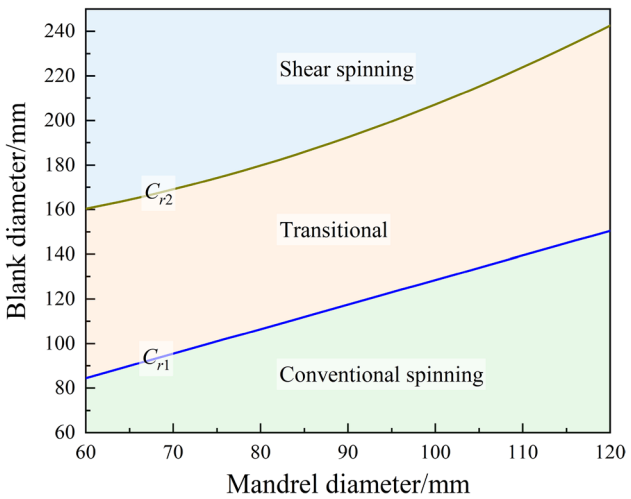

Fig. 14 Criterion of the initial forming state in die-less spinning

Table 4 Values of forming parameters

Forming parameters		Values
Blank parameters	Blank material	5052_s, **1060Al**, AlMg1SiCu_c
	Blank thickness (mm)	0.5, **1**, 1.5
Mold parameters	Roller diameter (mm)	200, **250**, 300
	Roller corner radius (mm)	2, **4**, 6
Process parameters	Feed ratio (mm/r)	0.5, **1**, 1.5
	Half cone angle (°)	40, **50**, 60

The bold values are the default values of the forming parameters in FE simulations

Table 5 Mechanical properties of 5052_s and AlMg1SiCu_c

Material	5052_s	AlMg1SiCu_c
Young's modulus/GPa	69.50	68.65
Poisson's ratio	0.33	0.30
Yield strength/MPa	67.00	98.07
Hardening index	0.15997	0.12200

similar to a quadratic curve. Therefore, the linear relationship and quadratic polynomial are selected to fit the relationship between critical values and general mandrel diameter. And the fitting equations are shown below:

$$C_{r1} = 18.5 + 1.1d_m \tag{1}$$

$$C_{r2} = 150.2 - 0.43d_m + 0.01d_m^2 \tag{2}$$

where d_m is the diameter of the mandrel.

In addition, the critical value at the general mandrel diameter of 90 mm in Fig. 11 is used to verify the accuracy of the fitting equations (Table 3). The prediction result shows that the prediction value of the fitting equations agrees well with the measurement value of the FE model: the prediction relative errors for C_{r1} and C_{r2} are 0.43% and 0.78%, respectively, which indicates that the fitting equations are accurate enough to serve as the criterion for the initial forming state. On the condition that the diameter of the general mandrel is known, the initial forming state during the die-less spinning process can be determined by Fig. 14: conventional spinning state when the blank diameter is smaller than C_{r1}; transition state when the blank diameter is between C_{r1} and C_{r2}; and shear spinning state when the blank diameter is larger than C_{r2}.

3.3 Effects of forming parameters on the criterion for the initial forming state

From the above analyses, it can be concluded that the blank diameter and general mandrel diameter are the main parameters affecting the initial forming state in die-less spinning. In addition, other forming parameters may also influence the initial forming state (Table 4). These parameters could be divided into blank parameters, mold parameters, and process parameters. Determining the dependence of initial forming state criterion on these parameters is critical to realize the control of forming quality. So, single-factor experiments for different parameters are conducted here to study the effects of spinning parameters on the criterion when the diameters of the blank and mandrel are 220 mm and 90 mm. Similar to the method in Sect. 3.2, FE simulations with variable intervals of mandrel diameter are carried out to obtain the criterion values C_{r1} and C_{r2}. The values of forming parameters are shown in Table 4. When a parameter is to be analyzed, the values of other parameters are set as the bold values in Table 4. In addition, the blank material is considered an investigation variable, and the mechanical properties

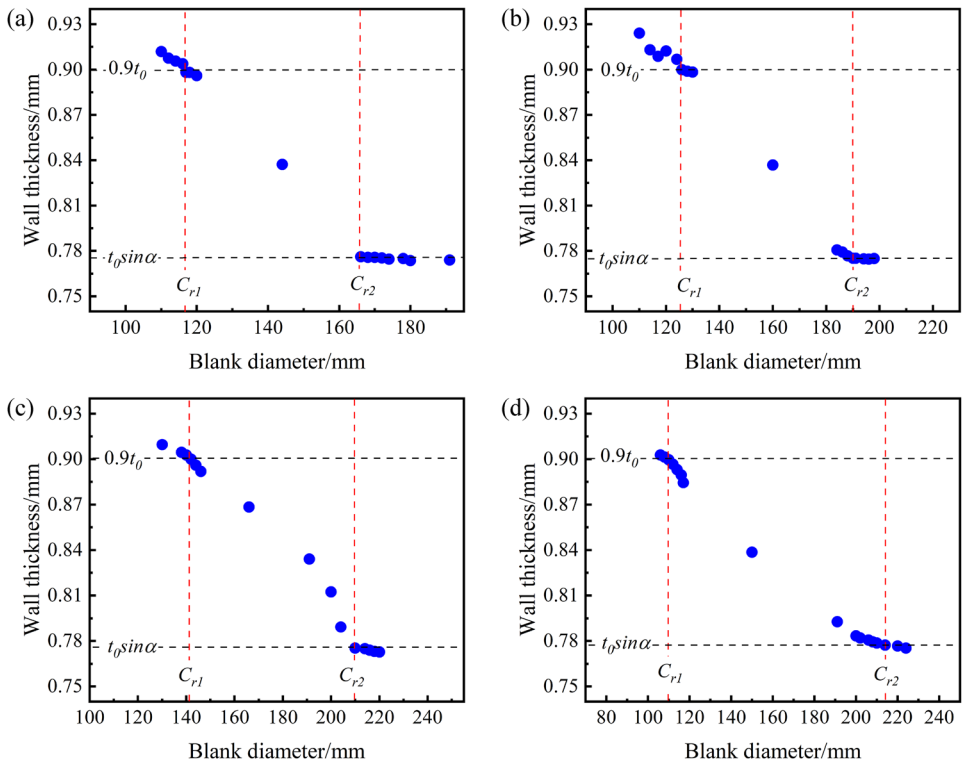

Fig. 15 Variation in formed wall thickness at the initial forming state with blank diameter in die-less spinning of different materials: **a** 5052_s; **b** AlMg1SiCu_c and different blank thicknesses: **c** 0.5 mm; **d** 1.5 mm

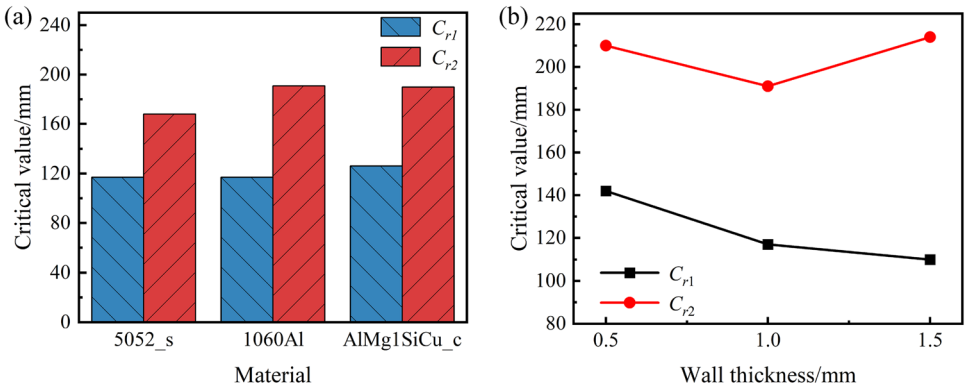

Fig. 16 Effect of material (**a**) and blank thickness (**b**) on the initial forming state criterion

(Table 5) are measured by the uniaxial tensile tests at room temperature using the CMT5205 universal testing machine.

Figure 15 shows the variation in the formed wall thickness with the blank diameter under different material and blank parameters. They all present the same variation trend as that in Fig. 11. C_{r1} and C_{r2} for different materials, and different initial blank thicknesses are obtained from Fig. 15 and then shown in Fig. 16. From Fig. 16a, it can be seen that the material mechanical properties have a certain effect on the initial forming state criterion. Meanwhile, the result in Fig. 16b reveals that with the increase in initial blank thickness, the criterion C_{r1} decreases, while C_{r2} decreases and then increases.

Figure 17 shows the variation in the formed wall thickness at the initial forming state with the blank diameter under different roller diameters and roller corner radius, and Fig. 18 shows the effect of the roller diameter and roller corner radius on the initial forming state criterions. From Fig. 18a, it can be seen that a larger roller diameter can improve the value of C_{r1} and has little effect on the value of C_{r2}. For different roller corner radius, Fig. 18b reveals that there is a positive relationship between the criterial values and roller corner radius. Furthermore, the C_{r1} increases linearly with increasing roller corner radius, while C_{r1} remains constant first and then increases with increasing roller corner radius.

Figures 19 and 20 show the variation in formed wall thickness at the initial forming state with the blank diameter under different feed ratios and half-cone angles and their effects on forming state criterions. It can be seen from Fig. 20a that both C_{r1} and C_{r2} increase with increasing roller

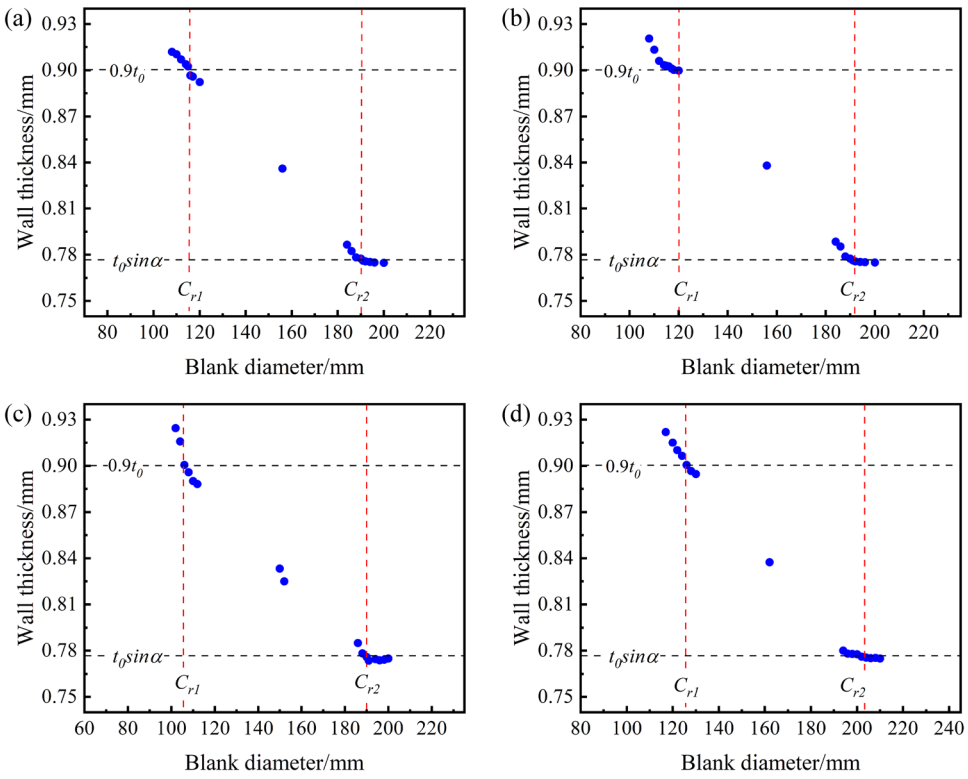

Fig. 17 Variation in formed wall thickness at the initial forming state with blank diameter in the die-less spinning process of different roller diameters: **a** 200 mm; **b** 300 mm and different roller corner radius: **c** 2 mm; **d** 6 mm

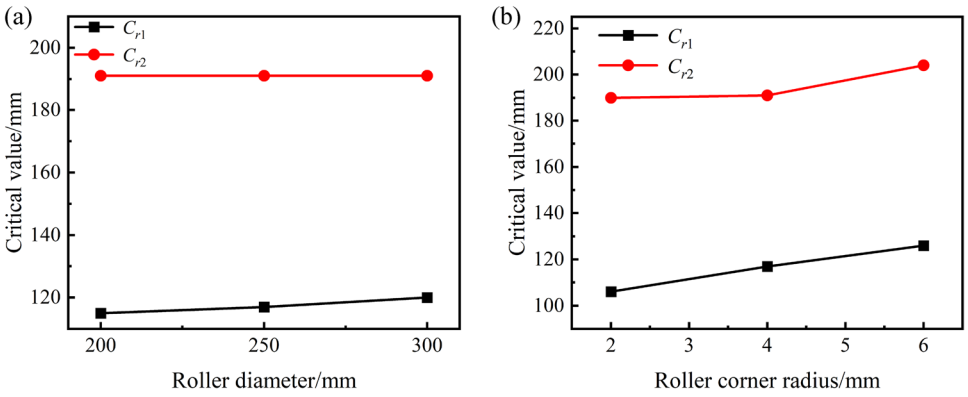

Fig. 18 Effect of roller diameter (**a**) and roller corner radius (**b**) on the initial forming state criterion

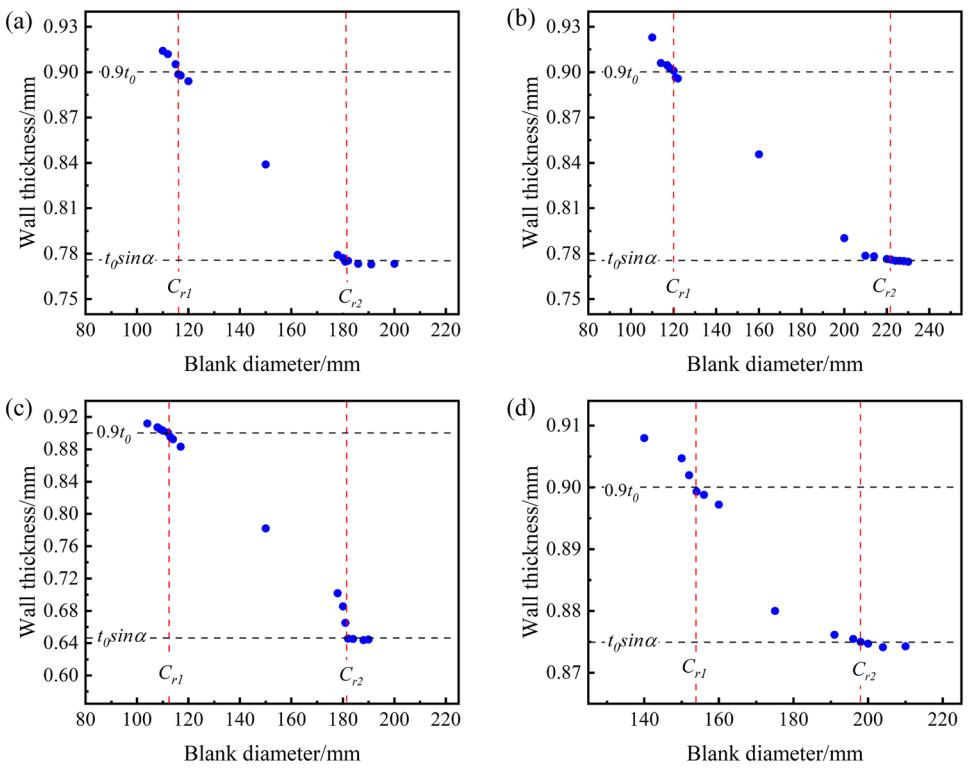

Fig. 19 Variation in formed wall thickness at the initial forming state with blank diameter in the die-less spinning process of different feed ratios: **a** 0.5 mm/r; **b** 1.5 mm/r and different half-cone angles: **c** 40°; **d** 60°

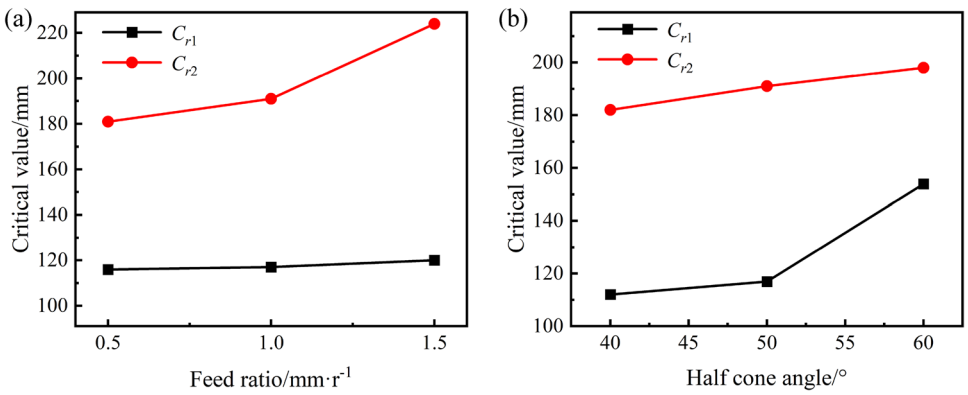

Fig. 20 Effect of the feed ratio (**a**) and half cone angle (**b**) on the initial forming states criterion

feed ratio, and C_{r2} increases more greatly than C_{r1}. Thus, the feed ratio has a greater effect on C_{r2} than on C_{r1}. The result in Fig. 20b reveals that there is a positive relationship between the criterions and half-cone angle.

4 Conclusion

In this study, the forming states in die-less spinning are analyzed. In addition, a criterion for the forming states is established, and its dependence on the forming parameters is also analyzed. The conclusions can be summarized as follows:

1. In die-less spinning, the formed wall thickness gradually increases with the spinning process. According to the wall thickness variation degree, three forming states are defined: shear spinning state ($t_f = t_0 sin\alpha$, where t_0 and t_f are the initial and formed wall thickness, respectively, and α is half-cone angel), conventional spinning state ($t_f > 0.9t_0$), and transition state between the shear and conventional spinning states ($t_0 sin\alpha < t_f \leq 0.9t_0$). Ther shear spinning state presents severe radial tension and thickness compressive stress and strain in the roller action area, while almost no stress and strain occur in the flange area; the conventional spinning state presents a large circumferential compressive stress and strain in both the roller action and flange area; the transition state between the shear and conventional spinning states presents similar and more slight deformation than the conventional spinning state.
2. The die-less spinning always proceeds in the sequence of shear spinning state, transition state, and conventional spinning state, while the initial forming state may be any one of them. It can be said that the evolution of forming states in die-less spinning could be determined by the initial forming state: when the initial forming state is conventional spinning state, the spinning process will be under conventional spinning state all the time; when the initial forming state is transition state, the spinning process will contain the transition state and conventional spinning state; and the spinning process will undergo all three states when the initial forming state is shear spinning state.
3. The initial forming state is mainly determined by the diameters of the blank and general mandrel. At a certain general mandrel diameter, the initial forming state changes from the conventional spinning state to the transition state and then the shear spinning state with increasing blank diameter. Moreover, the critical blank diameter between the conventional spinning state and transition state (noted as C_{r1}) changes linearly with the variation in the general mandrel diameter; the variation in the critical blank diameter between the transition state and shear spinning state (noted as C_{r2}) with the general mandrel diameter presents quadratic curve. On these bases, a criterion for the initial forming state is developed by modeling C_{r1} and C_{r2} as a function of the general mandrel diameter.
4. The influence of the die-less spinning forming parameters on the initial forming state criterion is studied. It is found that material parameters have a certain effect on both C_{r1} and C_{r2}, and roller diameter has no effect on C_{r2}. With the increase of initial blank thickness, criterion C_{r1} presents a decreasing trend, and criterion C_{r2} first decreases and then increases. Criterion C_{r1} increases with increasing roller corner radius, feed ratio, and half cone angle. The criterion C_{r2} increases with increasing roller diameter, roller corner radius, feed ratio, and half cone angle.

Author contribution Xinggang Yan: conceptualization, methodology, investigation, experiments, software, writing—original draft. Mei Zhan: writing—review and editing, supervision, project administration, funding acquisition. Yao Wang: investigation, experiments, resources. Pengfei Gao: conceptualization, supervision, writing—review and editing, funding acquisition. Yongdi Wang: software, data curation.

Funding This work was supported by the National Key R&D Program of China (Grant number 2020YFA0711100), the National Natural Science Foundation of China (Grant numbers 92060107 and 51875467) and the National Science and Technology Major Project (Grant number J2019-VII-0014–0154).

Data availability Not applicable.

Declarations

Ethical approval Not applicable.

Consent to participate Not applicable.

Consent for publication All the authors have read and agreed to the published version of the manuscript.

Competing interests The authors declare no competing interests.

References

1. Kwiatkowski L, Tekkaya AE, Kleiner M (2013) Fundamentals for controlling thickness and surface quality during dieless necking-in of tubes by spinning. CIRP Ann 62(1):299–302. https://doi.org/10.1016/j.cirp.2013.03.054
2. Xia QX, Xiao GF, Long H, Cheng XQ, Sheng XF (2014) A review of process advancement of novel metal spinning. Int J Mach Tool Manufact 85:100–121. https://doi.org/10.1016/j.ijmachtools.2014.05.005
3. Music O, Allwood JM, Kawai K (2010) A review of the mechanics of metal spinning. J Mater Process Technol 210(1):3–23. https://doi.org/10.1016/j.jmatprotec.2009.08.021
4. Wang CH, Liu KZ, Zhou L (2017) Xuan Ya Ji Shu (in Chinese). Fujian Science and Technology Publishing House, Fuzhou

5. Sugita Y, Arai H (2014) Formability in synchronous multipass spinning using simple pass set. J Mater Process Technol 217:336–344. https://doi.org/10.1016/j.jmatprotec.2014.11.017
6. Zhang JH, Zhan M, Yang H, Jiang ZQ, Han D (2012) 3D-FE modeling for power spinning of large ellipsoidal heads with variable thicknesses. Comp Mater Sci 53(1):303–313. https://doi.org/10.1016/j.commatsci.2011.08.010
7. Guo H, Wang J, Lu GD, Sang ZH, Wang QH (2017) A study of multi-pass scheduling methods for die-less spinning. J Zhejiang Univ - Sci 18(6):413–429. https://doi.org/10.1631/jzus.A1600403
8. Gao PF, Yan XG, Li FG, Zhan M, Ma F, Fu MW (2022) Deformation mode and wall thickness variation in conventional spinning of metal sheets. Int J Mach Tool Manufact 173:103846. https://doi.org/10.1016/j.ijmachtools.2021.103846
9. Wang L, Long H (2013) Roller path design by tool compensation in multi-pass conventional spinning. Mater Des 46:645–653. https://doi.org/10.1016/j.matdes.2012.10.048
10. Li ZX, Shu XD (2019) Numerical and experimental analysis on multi-pass conventional spinning of the cylindrical part with GH3030. Int J Adv Manuf Technol 103(5–8):2893–2901. https://doi.org/10.1007/s00170-019-03767-2
11. Tokuhiro S, Suzuki N, Takeuchi O (2018) Cylinder forming by die-less shear spinning with sheet thickness controlling of its wall. Procedia Manuf 15:1232–1238. https://doi.org/10.1016/j.promfg.2018.07.364
12. Gondo S, Arai H, Kajino S, Nakano S (2021) Evolution of strain state of a rolled aluminum sheet in multi-pass conventional spinning. J Manuf Sci Eng Trans ASME 143(6):061011. https://doi.org/10.1115/1.4049476
13 Bai DN, Gao PF, Yan XG, Wang Y (2021) Intelligent forming technology: state-of-the-art review and perspectives. J Adv Manuf Sci Technol 1(3):2021008. https://doi.org/10.51393/j.jamst.2021008
14. Chen SW, Gao PF, Zhan M, Ma F, Zhang HR, Xu RQ (2018) Determination of formability considering wrinkling defect in first-pass conventional spinning with linear roller path. J Mater Process Technol 265:44–55. https://doi.org/10.1016/j.jmatprotec.2018.10.003
15. Kang DC, Wang ZR, Li SD, Cheng QM (1985) Spinning of cone without mandrel (in Chinese). China Metal Form Eq Manuf Technol 03:13–17
16. Kang DC, Wang ZH (1999) Study on deformation mode of conventional spinning of plates. J Mater Process Technol 91(1–3):226–230. https://doi.org/10.1016/S0924-0136(98)00447-6